Influence of strain rate and temperature on the deformation mechanisms of a fine-grained Ti-6Al-4V alloy

Laurie Despax, Vanessa Vidal, Denis Delagnes, Moukrane Dehmas, Hiroaki Matsumoto, Vincent Velay

Influence of strain rate and temperature on the deformation mechanisms of a fine-grained Ti-6Al-4V alloy

Laurie Despax[a,*], Vanessa Vidal[a], Denis Delagnes[a], Moukrane Dehmas[b], Hiroaki Matsumoto[c], Vincent Velay[a]

[a] *Institut Clément Ader (ICA), Université de Toulouse, CNRS, IMT Mines Albi, UPS, INSA, ISAE-SUPAERO, Campus Jarlard, 81013 Albi CT Cedex 09, France*
[b] *CIRIMAT, Université de Toulouse, CNRS, 4 allée Emile Monso, BP 44362, 31030 Toulouse Cedex 04, France*
[c] *Department of Advanced Materials Science, Faculty of Engineering, Kagawa University, 2217-20 Hayashi-cho, Takamatsu, Kagawa 761-0396, Japan*

Abstract

Depending on their initial microstructure, titanium alloys, as the Ti-6Al-4V may have activation of different deformation mechanisms during hot forming processes. In this work, interrupted tensile tests and heat treatments are used to improve the understanding of the mechanical and microstructural behaviour of a fine-grained Ti-6Al-4V alloy at two temperatures (750 °C and 920 °C) and so for two different β phase fractions. The microstructural features like, α grain size and phase fraction, were determined by Scanning Electron Microscope (SEM) and image analysis. Moreover, evolution of the preferred crystallographic orientation of α grains and local misorientations between and inside grains were obtained by Electron Backscatter Diffraction (EBSD). The strain rate sensitivity parameter as well as the activation energy were deduced from mechanical tests. It appears, from all these microstructural and mechanical data, that several mechanisms are activated depending on the strain level and on the temperature range. At 750 °C, for a high strain rate, the deformation is mainly controlled by dislocations activity in the α phase (texture changes, dynamic recrystallization) and, at very low strain rate, by probably GBS accommodated with dislocations activity into α (recovery) and β. On the contrary at 920 °C, a clear decrease of the overall texture intensity associated with a high m value suggests that GBS is the dominant mode of deformation. Nevertheless, as the α/β volume fraction is around 48 %/52 % at this temperature, not only the α phase but also the β phase as well as α/α and β/β boundaries might contribute to the flow behaviour. During long deformation time (low strain rate and high temperature), dynamic coarsening behaviour (both into α and β), that is controlled by bulk diffusion, can occur and modify the type, the distribution and decrease the number of α/β, α/α and β/β boundaries. This can be partly related to the flow hardening observed at 920 °C and $10^{-4}\,s^{-1}$.

*Corresponding author
Email address: ldespax@mines-albi.fr (Laurie Despax)

Keywords:
Titanium alloys, Mechanical behaviour, Superplasticity, Interrupted tensile test, Texture, β-phase, Electron backscatter diffraction (EBSD).

1. Introduction

Titanium alloys are widely used in the aerospace industry as they combine a good resistance to corrosion and good mechanical properties as their strength to weight ratio and good ductility [1]. They are also known to have interesting superplastic behaviour. Indeed, superplastic forming (SPF) process uses the ability of some materials to withstand a huge deformation without necking at high temperature ($T > 870\,°C$) and low strain rate ($10^{-4}\,s^{-1}$) to produce near net shape parts. Moreover it is commonly admitted that a fine-grained ($d_\alpha < 10\,\mu m$) and equiaxed microstructure of two-phase titanium alloys (e.g Ti-6Al-4V) would promote this superplastic behaviour at intermediate temperatures (650 °C-800 °C) [2].

Since the last thirty years, some researches concentrate on investigating the ways to improve the cost efficiency of SPF [3, 4] by reformulating the alloy chemistry [5] or by decreasing the temperature as well as the forming time. The refinement of the initial microstructure (grain size lower than 10 µm) appears to be a promising way [6, 7]. During SPF, the involved deformation mechanisms can be significantly different depending on the temperature (and so the phase fraction α/β), the strain rate and so the initial microstructure [8]. For two-phase titanium alloys such as the Ti-6Al-4V, the deformation is mainly described as being controlled by either the α phase (isostrain-rate mode) [9], the β phase (isostress mode) [9] or controlled by a competition between the two ones [9, 10]. In addition to the description of the role of each phase, the mechanisms at high temperatures are generally described in terms of dislocations climb [11], diffusional creep [12], grain boundary sliding (GBS) supported by several accommodation mechanisms like vacancy diffusion or dislocations glide [13] as well as microstructural changes (dynamic recrystallization, grain growth and grain rotation).

The understanding of the deformation mechanisms involved in superplastic forming (SPF) remains a major challenge because each study shows as many mechanisms as experimental conditions and is mainly based on the analysis of stress-strain curves [10] or on the post mortem characterization of samples [8, 9, 14]. As an example, in the case of a Ti-6Al-4V alloy with an α grain size of 6 µm, at 900 °C, Alabort et al. suggested, by in-situ SEM observation, a mechanism of GBS completed by the motion of dislocations in the β phase, which seems to be dependent on the β grain size [15]. Kim et al. proposed a phase boundary sliding (PBS) rather than GBS due to the presence of dislocations only at α/β interfaces [9]. In the temperature range of 750 °C-850 °C and for an initial α grain size about 5 µm, Yang et al. described a mechanism involving GBS combined with a stress softening explained by dynamic recrystallization for the lowest temperatures and a strain hardening noticeable by an α grain growth for the highest temperatures [14]. These studies are mainly based on mechanisms identified in the α phase. However, the phase fractions and the number of α/β interfaces might be different at high temperature and so may influence the mechanical behaviour. An increase of the β phase fraction seems to favour the GBS by enhancing the mechanisms of accommodation [10, 14, 15]. Furthermore, the understanding of mechanisms at

high temperatures ($> 900\,°C$) is poorly documented because they are too far from industrial superplastic favourable conditions [8, 16]. Liu et al. described a mechanism of GBS controlled by lattice diffusion at 890 °C with a high strain rate. By applying high temperatures, the dislocations mobility is favoured leading to the formation of large grain boundaries and thus to a grain boundary slip [17].

Thus, although there are several papers dealing with the mechanisms of SPF in titanium alloys, there is not much literature on superplastic deformation mechanisms in Ti-6Al-4V alloys with a grain size below 4 µm and for temperatures above 900 °C. These considerations motivate the current study to improve the understanding of deformation mechanisms involved in a fine-grained Ti-6Al-4V alloy (d_α= 2 µm), for two strain rates ($10^{-2}\,s^{-1}$ and $10^{-4}\,s^{-1}$) and two temperatures (750 °C and 920 °C) for which the β phase fraction is significantly different. Therefore, interrupted tensile tests and SEM-EBSD characterizations were carried out to study the mechanical behaviour and the microstructural evolution (α phase fraction, α grain size and crystallographic orientation) at each deformation step. This paper provide, thus, a better understanding on how a fine grain size can significantly modify the value of the optimal α/β phase fraction ratio (classically reported around 40-50% for superplasticity) and, so, the mechanisms of superplasticity. Moreover, a special effort have been made at high temperature to discuss the mechanisms that could coutribute to the hardening.

2. Materials and Methods

The material investigated in this study, supplied by Airbus France, is a fine-grained (FG) Ti-6Al-4V alloy in the shape of 3 mm thick sheets processed by rolling and by a heat treatment at 770 °C during 40 min followed by air cooling. The nominal chemical composition (wt.%) of this alloy was 6.26 Al, 3.92 V, 0.33 O, 0.24 Fe, 0.01 C and 0.01 N. The β-transus temperature is around 1000 °C. Pole figures for five lattice plan hkl reflections were obtained with a X-ray diffractometer (X'Pert PANALYTICAL) by using an Euler cradle. Phi angles were measured between 0° and 360° each 5° for 150 s. Psi angles were obtained with a rotation from 0° to 70° each 5°. The "X'Pert Texture"software was thus used to calculate pole figures.

Flow behaviour at high temperatures (750 °C and 920 °C) and at two constant strain rates ($10^{-2}\,s^{-1}$ and $10^{-4}\,s^{-1}$) was characterized by tensile test measurements performed with a servo-hydraulic testing machine and a three-zones furnace to minimize the temperature gradient on the specimen during deformation. The temperature on each zone of the furnace was controlled by K-thermocouples positioned in the centre of each zone (Fig.1). Dog bone specimens (gauge section of $3 \times 8\,mm^2$, a gauge length of 15 mm and a tensile axis parallel to the rolling direction) were machined (see Fig.1(b) which shows the shape, dimensions and sample coordinate system (ND, TD and RD mean respectively Normal, Transverse and Rolling Directions)). As titanium alloys are sensitive to oxidation, the samples were placed in a quartz tube with a constant argon flow. The heating rate was $10\,°C\,min^{-1}$ followed by an isothermal holding time of 15 min at the desired temperature before starting the tensile test. At the end of the mechanical loading, the samples were cooled down to the room temperature inside the furnace. Therefore, α grain size data should be used with caution, as a growth regime can be certainly activated during this cooling.

To correlate the microstructural evolution with the plastic strain level, interrupted tensile tests were performed. So for each tensile test conditions (temperature and strain rate), at least three samples, characterized each by a different incremental strain level, were obtained. Then the evolution of the microstructure was conducted on these samples deformed to different strain levels, to provide data about the involved deformation mechanisms. In the following sections, results of these characterizations are reported. Note that some cautions have to be taken while interpreting these data due to the slow cooling used from the test to ambient temperature. In particular, due to the grain growth mechanisms that could occur during slow cooling, it is assumed that (i) the measured α grain size at room temperature is surely slightly higher than before cooling, (ii) there is no noticeable modification of the crystallographic orientation of the α phase while cooling by considering that there is no nucleation processes involved [18].

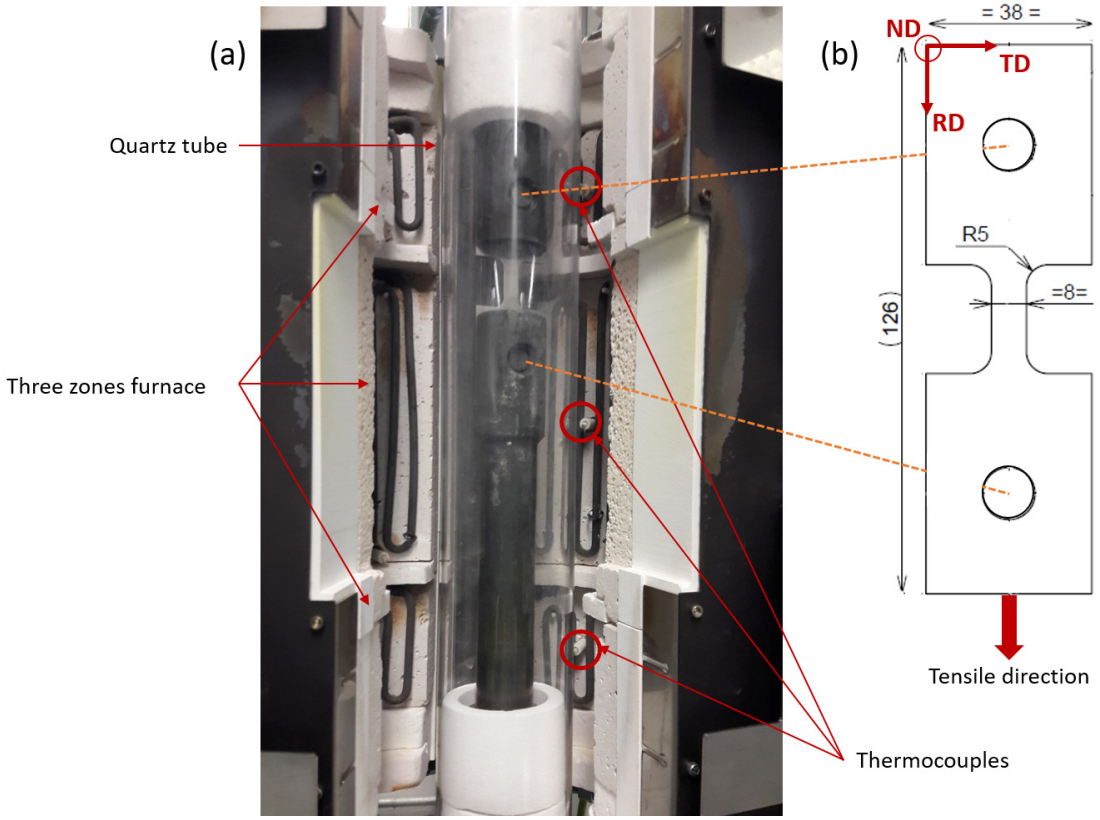

Figure 1: (a) Servo-hydraulic testing machine with a three zones furnace and a quartz tube to have an argon atmosphere. Red circles show the thermocouples used to control the temperature of the furnace. (b) Details of the dimensions of the tensile test sample in millimeter and the tensile direction parallel to the rolling direction.

Complementary tensile tests were done at 870 °C, 900 °C and with a strain rate of $10^{-3}\,s^{-1}$ to evaluate the strain rate sensitivity m. Indeed, this parameter expresses the sensitivity of the stress to the strain rate and requires at least three temperatures and strain rates to

be calculated. It was determined by evaluating the slope of the $\ln(\sigma)$-$\ln(\dot{\varepsilon})$ curves at a logarithmic strain of 0.4 (Eq.1).

$$\dot{\varepsilon} = A\sigma^{\frac{1}{m}} \tag{1}$$

Heat treatments were also performed to study the phase transformations occurring during heating and isothermal holding without mechanical loading contribution. So, the phase fraction evolution on heating was obtained from different heat treatments carried out with a resistive furnace using the following parameters: a heating rate of $10\,^{\circ}\mathrm{C\,min^{-1}}$, a holding time of 2 h at temperatures in the range of 765 °C to 935 °C, and a water quenching. Then to evaluate only the influence of the holding time at high temperature on the microstructural evolution (without mechanical loading), additional heat treatments were carried out at 920 °C using a radiative inert gas (Argon) furnace with two different holding times (20 min and 210 min) representative to the duration of the tensile tests (respectively test at $10^{-2}\,\mathrm{s^{-1}}$ and $10^{-4}\,\mathrm{s^{-1}}$). The applied heating rate is about $10\,^{\circ}\mathrm{C\,min^{-1}}$. The temperature was monitored with a thermocouple inside the furnace and not welded to the surface of the sample. The absolute error on the temperature in the range 750 °C – 950 °C was estimated to be ±20 °C. Samples were water quenched after the heat treatment.

For the microstructural and microtextural characterizations, the samples before and after hot deformation and heat treatment were polished using standard preparation. The final step was a prolonged polishing (about 10 min) using a colloidal silica suspension with 20 % of H_2O_2. Key microstructural features that are the α grain size (d_α) and the phase fraction (f_α/f_β) were determinated by image analysis (Aphelion® software) from images recorded using a scanning electron microscope (SEM - Novanosem450 FEI) in backscattered mode (BSE), operated at an accelerator voltage of 15 kV. The intercept method for the determination of the α grain size and the surface fraction were conducted on at least 15 images/sample. Incomplete pole figures of $\{10\bar{1}0\}_\alpha$ and $\{0001\}_\alpha$ reflections were measured on the initial material with a X-ray diffractometer (X'Pert Panalytical) equipped with an Euler cradle using a step size of 5°. The obtained data were processed by the software X'Pert Texture from Panalytical. Note that texture measurements by XRD were only performed on the initial material.

Moreover Electron Backscattering Diffraction (EBSD) analysis using a JEOL JSM-7001F field emission gun scanning electron microscope equipped with an Oxford-HKL electron backscatter diffraction detector was carried out to characterize the evolution of the local crystallographic orientation and the substructure evolution. 122 x 91 µm maps were made using a square grid at a step size of 0.3 µm for the temperature of 750 °C and 302 x 228 µm maps with a step size of 0.4 µm at 920 °C. The conditions were chosen according to the α grain size, which is higher at 920 °C. EBSD data were processed using two software, i.e. HKL Channel 5® (Oxford instrument) and TSL OIM 5 (TexSem). Both software were used because HKL Channel 5 is the processing software available in the Institut Clément Ader (ICA) laboratory and TSL is a software allowing easy manipulation of data concerning small misorientations. Indeed, it allows exporting these data in order to estimate the density of Geometrically Necessary Dislocations (GNDs) and to show them in the form of a map. To

describe the local misorientation within a grain, the Kernel Average Misorientation (KAM) parameter was used. It consists in the average misorientation between a point on the centre of a hexagonal measurement grid and the second nearest neighbours [19]. Note that boundaries with a misorientation angle (θ) higher than 15° are considered as high angle grain boundaries (HAGB) and in the range of 2° to 15° as sub-grain boundaries/low angle grain boundaries (LAGB).

3. Results

3.1. As-received state

Fig.2(a) shows a typical SEM-BSE image of the microstructure in the as-received state on the RD/TD surface that is assumed to be representative of the material. The α phase appears in black and the β phase in white (Fig.2(a)). The SEM micrograph reveals an initial heterogeneous microstructure with a mixture of equiaxed and slightly elongated α grains along the rolling direction with the β phase distributed along these α grains. The α phase amount was found to be about 87 ± 1 *vol.*%. EBSD data confirm that the morphology of α phase can be either nodular or slightly elongated with a size of about 2.1±0.7 µm and 7.7 ± 2.3 µm x 3.1 ± 1.1 µm (Fig.2(b),(c)), respectively.

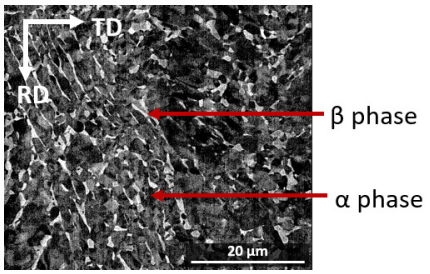

(a) SEM image

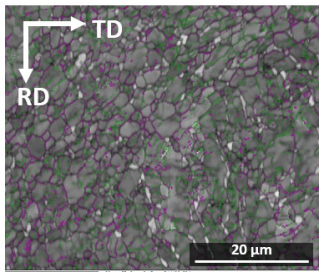

(b) EBSD/Grain boundaries map

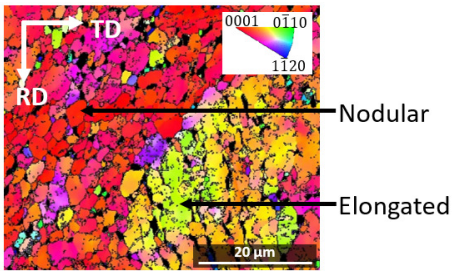

(c) EBSD/IPF-ZO map

Figure 2: As-received microstructure analysed by SEM-BSE on the RDTD plane with α phase in black and β phase in white (a), EBSD map (index quality on α representation of HAGB (misorientation>15° in purple) and LAGB (2°<misorientation<15° in green)) (b) and inverse pole figure according to Z0 normal direction to the sample surface (c).

Texture measurements done by X-Ray diffraction indicate an initial rolling texture with basal planes $\{0001\}_\alpha$ tilted by ± 25° from the normal direction toward the rolling direction

(Fig.3(a)) and with the normal of prismatic poles $\{10\bar{1}0\}_\alpha$ parallel to the transverse direction (Fig.3(c)). A slight tilt of the sample can also be revealed because the poles that would be expected at 75° are only visible on one side of the pole figure (Fig.3(b)). Because of the limited β phase volume fraction in the Ti-6Al-4V at room temperature, only limited EBSD results were obtained for this phase on the as-received Ti-6Al-4V sheet.

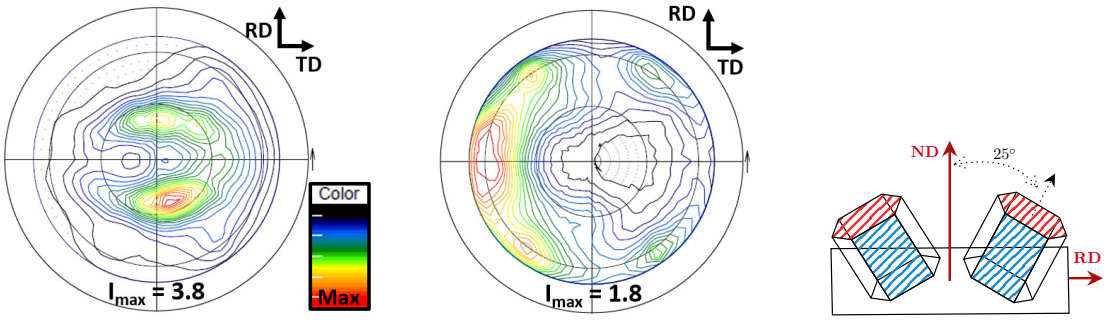

(a) $\{0001\}_\alpha$ (b) $\{10\bar{1}0\}_\alpha$ (c) α grains orientation

Figure 3: $\{0001\}_\alpha$ and $\{10\bar{1}0\}_\alpha$ pole figures of the as-received Ti-6Al-4V alloy in the RD/TD plane obtained by X-ray diffraction, respectively (a)(b), and a schema of the preferential orientation of the α phase as a function of the rolling direction (RD) of the sheet(c). The plan in red shows the basal plans $\{0001\}_\alpha$ and in blue, the prismatic plans $\{10\bar{1}0\}_\alpha$.

3.2. Dissolution of α phase

Fig.4 displays the evolution of α phase amount obtained by image analysis as a function of the temperature (heating rate of 10 °C min^{-1} and 2 h isothermal holding). As expected, the α phase amount decreases with increasing the temperature from around 87 vol.% at 765 °C to 39 vol.% at 935 °C. The α phase dissolution into β seems to start around 765 °C.

The experimental data were compared with the equilibrium α phase amount predicted using Thermo-Calc® software and the Saunders database for titanium systems [20, 21] (TTTI3) and the nominal chemical composition. The predictions are consistent with the experimental results for temperatures higher than 765 °C. It can be assumed that a holding time of 2 h at high temperature is enough to achieve an equilibrium phase fraction [22]. However, one can emphasize that the α phase amount at the as-received state is below the fraction expected at equilibrium (95% by calculation against 87% by image analysis). This difference could be linked to the last heat treatment applied during the manufacturing of the sheet. Indeed, the sheet was heated to 770 °C and then air cooled to room temperature. During the rapid cooling, only a small amount of β phase is transformed into α [23]. Therefore, the α phase fraction presents at room temperature will be lower than the fraction predicted by thermodynamics. Moreover, the beginning of the α phase dissolution and of the α → β transformation can be noticed above 750 °C.

Fig.5(a), (b) and (c) show typical SEM images recorded after water quenching from 750 °C - 2 h, 920 °C - 20 min and 920 °C - 210 min, respectively. At 750 °C, the microstructure after water quenching is assumed to be representative of the microstructure at this high

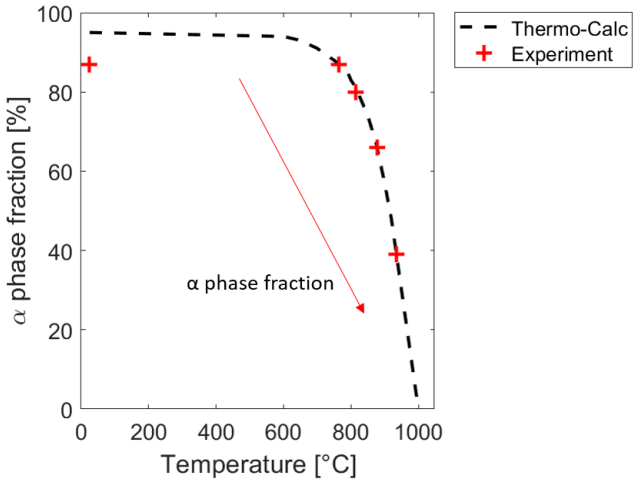

Figure 4: α phase fraction evolution as a function of the temperature at the as-received Ti-6Al-4V state obtained by image analysis on SEM-BSE images following the RD/TD plane.

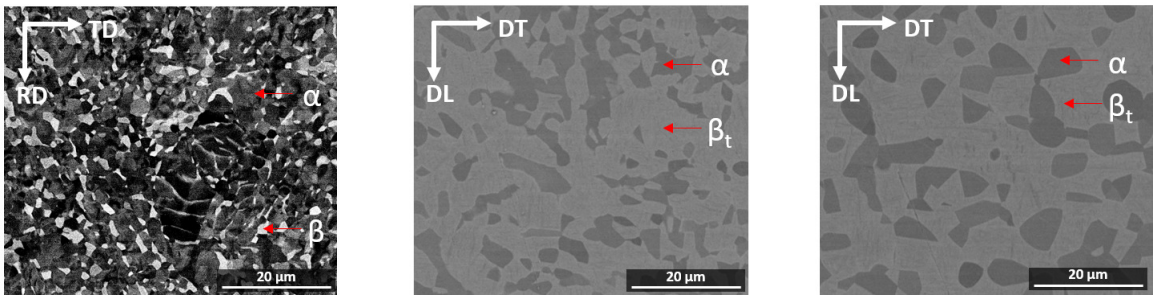

(a) 750 °C 120 min (b) 920 °C 20 min (c) 920 °C 210 min

Figure 5: SEM images obtained after water quenching from isothermal holding at high temperature: 750 °C for 120 min (a), 920 °C for 20 min (b) and 920 °C for 210 min (c).

temperature: the β phase appears in white (Fig.5(a)). Microstructure does not significantly differ from the as-received state. Indeed, at this temperature, the phase transformation has not yet started. However, there seems to be a slight change in the β phase distribution. On the contrary, during water quenching from 920 °C, the α' martensitic transformation from the decomposition of β phase occurred. The mixture of α' and β phases appears in light grey in SEM micrograph (Fig.5(b),(c)). As proved by Malinov et al. [22] and Dehmas et al. [24], the dissolution of the α phase into β phase is really fast (approximately <10 min). After heat treatment and quenching, the α phase amount was obtained to be about 33 vol.% for both holding times (20 min and 210 min). It is also noticed that the number density of α nodular grains measured by image analysis was found to be about 50 092 particles/mm^2 and 16 388 particles/mm^2 after 20 min and 210 min holding time, respectively. A difference on the α grain size was also observed with $d_\alpha = 3.2 \pm 1.1$ µm and $d_\alpha = 5.5 \pm 1.9$ µm after 20 min and 210 min holding time, respectively. The evolution of these microstructural features highlights a coarsening activation with the holding time at 920 °C [16].

3.3. Thermo-mechanical behaviour

Fig.6 represents the true stress and logarithmic strain curves obtained after tensile test at two temperatures (750 °C and 920 °C) and two strain rates ($10^{-2}\,s^{-1}$ and $10^{-4}\,s^{-1}$). Interrupted tensile tests for the further characterizations are represented by yellow cross symbols (Fig.6). The temperatures of 750 °C and 920 °C were chosen because the β phase fraction varies significantly and may have an impact on the mechanical behaviour: around 12 vol.% at 750 °C and 52 vol.% at 920 °C (Fig.4). It can be noticed that the stress-strain responses from interrupted tensile tests performed under the same conditions are, for the most part, comparable. Only a slight difference can be seen for the lower strain rate ($10^{-4}\,s^{-1}$) at 920 °C.

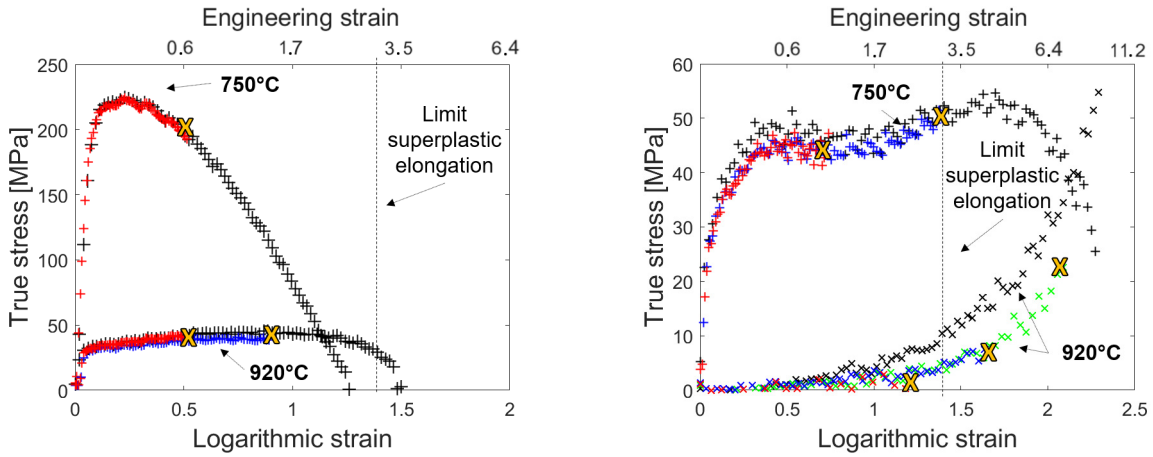

(a) $10^{-2}\,s^{-1}$ (b) $10^{-4}\,s^{-1}$

Figure 6: True stress and logarithmic strain curves obtained after tensile tests at 750 °C and 920 °C following two strain rates: $10^{-2}\,s^{-1}$ (a) and $10^{-4}\,s^{-1}$ (b). Yellow cross symbols are related to the interrupted tests for the further characterizations. Vertical dotted lines represent the minimum strain characteristics of a superplastic deformation.

Three different flow behaviours are mainly observed depending on the strain rate and the temperature: a softening of the stress, a steady state flow or a high hardening. The drop in stress level is mainly related to the necking of the sample. The condition at 920 °C-$10^{-4}\,s^{-1}$ is the only condition not to have been to failure. In the literature, a superplastic condition is defined by an elongation greater than 300% and a m value higher than 0.3 [25]. A superplastic elongation, which corresponds to an engineering strain greater than 300%, can be shown for each condition except the one with the highest strain rate and the lowest temperature. At high strain rate, the flow stress rapidly increases in the initial stage of deformation for the both temperatures. After the peak stress, the stress decreases (750 °C) or remains constant before slightly increasing (920 °C). At slow strain rate, at 750 °C, after an initial strain hardening and a slight softening, a steady-state flow characteristics of a superplastic flow occurs and is followed by a slight strain hardening and by a strain softening until the failure. At 920 °C, the stress-strain curves reveal a pronounced flow hardening with a low stress level on the first deformation stage.

3.4. Microstructural evolution during hot tensile test

3.4.1. Size and morphology of the α phase

Fig.7 shows the evolution of the α grain size determined by image analysis after interrupted tensile tests at different elongation levels for 750 °C (solid line) and 920 °C (dotted line) and for two strain rates: $10^{-2}\,s^{-1}$ (red symbols) and $10^{-4}\,s^{-1}$ (blue symbols).

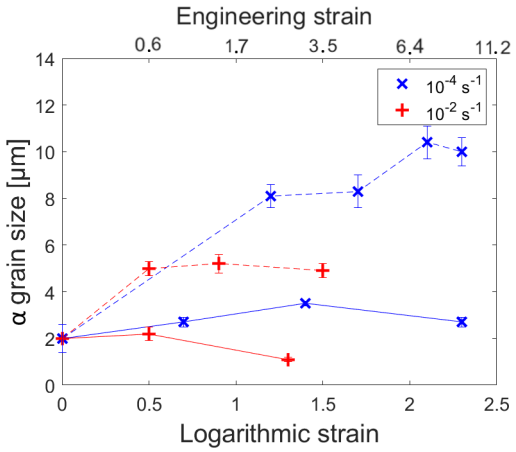

Figure 7: α grain size evolution after interrupted tensile test as a function of strain rate and temperature: 750 °C (solid line) and 920 °C (dotted line).

At 750 °C and for the highest strain rate ($10^{-2}\,s^{-1}$), no evident evolution of the α grain size is noticeable at low elongation level (corresponding to the beginning of the softening on the true stress and logarithmic strain curves in Fig.6), while a grain refinement is found to be at the failure. For the lowest strain rate ($10^{-4}\,s^{-1}$), the α grain size slightly increases until the maximum stress is reached. Then, a grain refinement occurs with less variation as compared to the higher strain rate. In addition, SEM images also reveal that the microstructure, initially heterogeneous in terms of the morphology, becomes equiaxed at the first step of deformation (Fig.8(a)). It can be also noticed that the β phase distribution, along the α grains, as well as its size seems to have changed (Fig.8(b) and 8(c)). As a function of the strain rate, a huge difference in the α grain size can be noticed. By looking to the evolution of the α grain size measured after interrupted tensile test (Fig.7), it can be observed that by increasing the temperature (920 °C), the α grain size increases compared to the ones obtained at 750 °C (Fig.9). The temperature as well as the time at high temperature might promote this effect. More specially, at $10^{-4}\,s^{-1}$, the grain size seems to continuously increase along the deformation with two drops around 250% and 600% of elongation (Fig.7, dotted blue line). On the contrary, at higher strain rate ($10^{-2}\,s^{-1}$), even if a high increase of the grain size occurs at the first step of deformation, then for higher elongation it almost remains the same (Fig.7, dotted red line). As mentioned, α grain shape is modified during deformation: (i) there is a modification as compared with the initial state, certainly due to a spheroidization or to a rearrangement of sub-grains into nodular grains [26], (ii) the grain shape is kept after deformation and failure, which is synonymous with superplastic deformation (no elongated grain morphology).

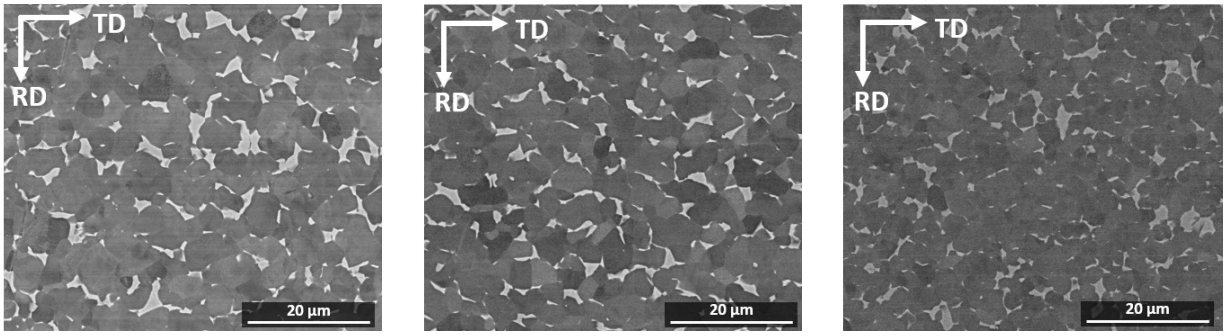

(a) 40% (b) 220% (c) 700%

Figure 8: SEM-BSE images after interrupted tensile test at different elongation levels for 750 °C and a strain rate of $10^{-4}\,s^{-1}$: 40% (a), 220% (b) and 700% (c) of engineering strain. (c) represents the microstructure at the failure. The α phase appears in dark and the β phase in light.

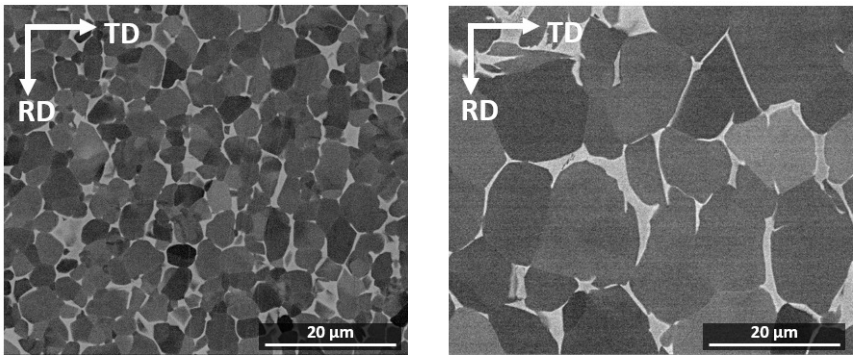

(a) 920 °C-$10^{-2}\,s^{-1}$ (b) 920 °C-$10^{-4}\,s^{-1}$

Figure 9: SEM-BSE images obtained after tensile test at 920 °C at two strain rates: $10^{-2}\,s^{-1}$(a) until the failure and $10^{-4}\,s^{-1}$(b) without failure. The α phase appears in dark and the β phase in light.

3.4.2. Crystallographic orientation of the α phase

Fig.10 displays the basal pole figures of the α phase obtained from EBSD measurements of samples at the initial state (Fig.10(a)) and after interrupted tensile tests at different elongation levels for 750 °C (Fig.10(b) to Fig.10(f)) and 920 °C (Fig.10(g) to Fig.10(m)) at two different strain rates. At 750 °C and for both strain rates, the crystal orientation of α grains gradually evolved: their basal planes tend to become parallel to the rolling direction (equal to the tensile direction). In addition, a decrease of the initial texture intensity is noticed at the first step of deformation in particular for the lowest strain rate (from $I_{max} = 9.5$ initially to 4.7 at $10^{-4}\,s^{-1}$).

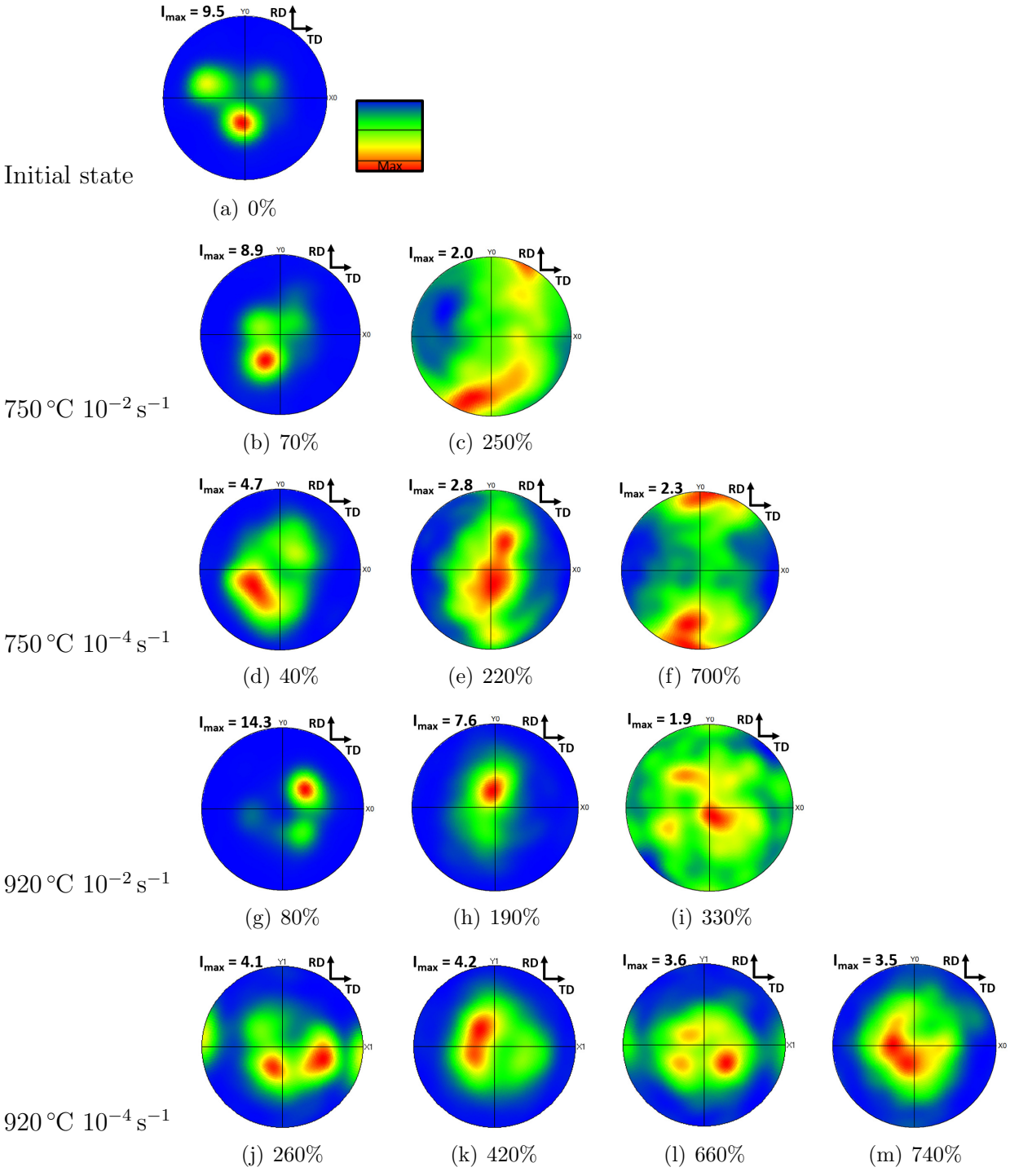

Figure 10: $\{0001\}_\alpha$ pole figures obtained by SEM-EBSD at the initial state (a) and after interrupted tensile tests at different elongation levels: 750 °C-10^{-2} s^{-1} (b,c), 750 °C-10^{-4} s^{-1} (d,e,f), 920 °C-10^{-2} s^{-1} (g,h,i) and 920 °C-10^{-4} s^{-1} (j,k,l,m). Each caption corresponds to the applied engineering strain and the pole figure intensity (higher diffraction probability density).

At 920 °C, $\{0001\}_\alpha$ basal pole figures mainly revealed a decrease of the initial texture component intensity that is related to a randomization of the α grains orientation. For the lowest strain rate, this decrease mainly occurs in early deformation stages ($I_{max} = 9.5$ initially to around 4) and afterwards the I_{max} value remains almost the same until the failure. On the contrary for the highest strain rate, I_{max} gradually decreases until reaching a small value at the fracture, revealing a strong randomization of the α grain orientation, which is widely associated with the grain boundary sliding mechanism. So while at 920 °C a randomization of the texture intensity was mainly observed, at lower temperature (750 °C), the deformation applied resulted in a modification of the preferential orientation of α grains. It could be then assumed that different mechanisms of deformation should be involved.

3.4.3. Substructure evolution: nature of grain boundaries and dislocations density estimation

The substructure evolution is shown in terms of LAGB and HAGB distribution as well as local misorientation that can be related to dislocations density evolution (by using KAM maps). The distribution of LAGB ($< 15°$) and HAGB ($\geq 15°$) is shown in Fig.11 for each temperature/strain rate condition.

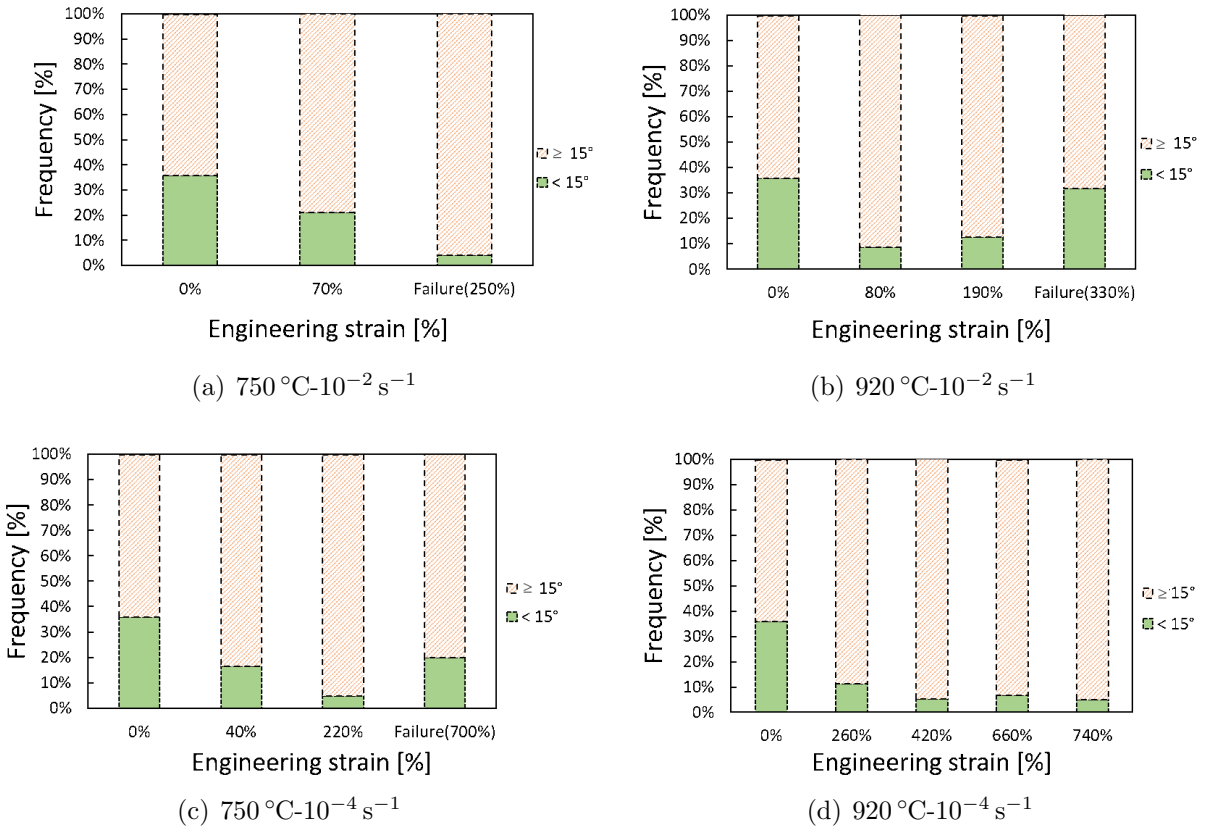

(a) 750 °C-10^{-2} s^{-1} (b) 920 °C-10^{-2} s^{-1}

(c) 750 °C-10^{-4} s^{-1} (d) 920 °C-10^{-4} s^{-1}

Figure 11: Misorientation distribution obtained by SEM-EBSD after interrupted tensile tests at different elongation levels: for two temperatures (750 °C (a,c)-920 °C (b,d)) and two strain rates (10^{-2} s^{-1} (a,b)-10^{-4} s^{-1} (c,d)).

During tensile test at 750 °C and for the highest strain rate (Fig.11(a)), the fraction of LAGB progressively decreases in favour of HAGB. For the lower strain rate, almost the same evolution is observed (Fig.11(c)), except before failure (so at the higher elongation) where the fraction of LAGB increases. At 920 °C, a high decrease of the LAGB clearly occurred in early deformation stages for both strain rates. Then, for the highest strain rate, an increase of the fraction of LAGB is progressively observed while the low fraction of LAGB remains almost the same until the fracture at low strain rate. As it can be assumed that these mechanisms are closely related to the dislocations activity, the density of geometrically necessary dislocations ($\bar{\rho}_{\mathrm{GND}}$) from the Kernel Average Misorientations (KAM) values was estimated. This parameter can be related to the local lattice curvature caused by dislocations and so to the evolution of intragranular substructures. Fig.12 shows the KAM evolution at different elongation levels for each condition. The hatched area represents the accuracy limit of the EBSD method. Indeed, due to its angular resolution, misorientation values of subgrain boundaries less than or equal to 0.5° are not considered.

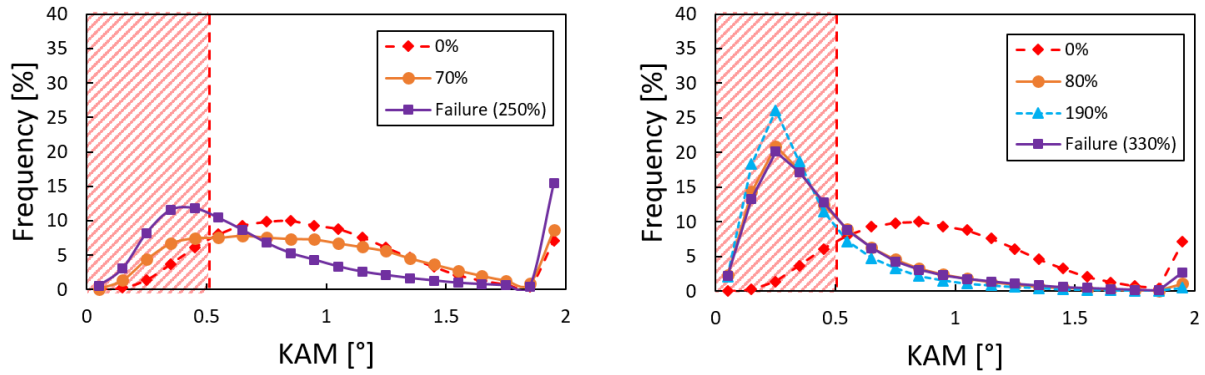

(a) 750 °C-10^{-2} s^{-1} (b) 920 °C-10^{-2} s^{-1}

(c) 750 °C-10^{-4} s^{-1} (d) 920 °C-10^{-4} s^{-1}

Figure 12: Kernel Average Misorientation (KAM) obtained from EBSD map for two temperatures (750 °C (a,c)-920 °C (b,d)) and two strain rates (10^{-2} s^{-1} (a,b)-10^{-4} s^{-1} (c,d)). The hatched area represents the accuracy limit of the EBSD method.

The KAM mean value of the as-received state is around 0.9° with a spread curve over

the KAM misorientation range. When the peak width is large, this reflects a high local plasticity in the grains and certainly a high dislocations density within the α grains [27]. It is possible to notice that overall, for low temperatures, the peak width greatly varies. In contrast to high temperatures, where the average KAM value decreases during the first deformation step and seems to be no longer modified. This decrease is described in the literature [27] as corresponding to the material recovery at high temperature. For the lowest temperature (750 °C) with the highest strain rate, the KAM distribution tends to spread when the deformation increases to 70%. However, the KAM mean value tends to decrease after failure. This could be explained by the rearrangement of dislocations in α grains into subgrain boundaries certainly linked with the influence of dynamic recrystallization. At the same temperature with a slow strain rate, the KAM mean value tends to decrease, as observed at high temperatures. This could mean that there is a lower dislocations activity in the α phase at this deformation stage. Then at the failure, the KAM curve seems to spread over a wider values range, maybe due to an accumulation of dislocations into the α phase at the failure.

In order to get the spatial distribution of the dislocations density for each condition, the density of geometrically necessary dislocations ρ_{GND} was calculated considering the Eq.2 established by Ashby [28].

$$\rho_{\mathrm{GND}} = \frac{2\Delta\theta}{b.d} \tag{2}$$

Where ρ_{GND} is the GND density, $\Delta\theta$ is the KAM value (rad), b is the burger's vector of the α phase ($b_{<11\bar{2}0>} = 2.95.10^{-10}$ m) and d is the step size used during the EBSD data acquisition. Calculated values are then used in the TLS software to obtain a GND density map.

Fig.13 shows the dislocations density maps in the α phase and corresponding mean values, calculated with Eq.2, at the as-received state and for different conditions. At the as-received state, the plastic strain seems accumulated, with an important dislocations density ($\bar{\rho}_{\mathrm{GND}} = 7.3 \times 10^{14}\,\mathrm{m}^{-2}$), in the α phase. At lower temperature and strain rate, the dislocations density seams localised at interfaces α/α and α/β during the deformation certainly due to a rearrangement of dislocations (Fig.13(c)). Then, at failure, the GND density heterogeneously increases in the α phase, certainly linked to dislocations activity favoured in some nodules after the grain growth observed (Fig.13(d)). At higher temperature and strain rate and from at least 80% of deformation, the dislocations density and distribution in the α phase almost remains the same until the failure. At 920 °C but for a lower strain rate, Fig.13(b) shows a contrast of dislocations density between the α phase and the grain boundaries. These results show a high dislocations activity in the α phase at 920 °C $10^{-2}\,\mathrm{s}^{-1}$ ($\bar{\rho}_{\mathrm{GND}} = 2 \times 10^{14}\,\mathrm{m}^{-2}$) whereas at 920 °C $10^{-4}\,\mathrm{s}^{-1}$, a lower dislocations activity in the α phase can be seen after the first step of deformation ($\bar{\rho}_{\mathrm{GND}} = 1.1 \times 10^{14}\,\mathrm{m}^{-2}$). The conditions 750 °C $10^{-4}\,\mathrm{s}^{-1}$ and 920 °C $10^{-2}\,\mathrm{s}^{-1}$ seem to have a similar modification of the substructure in the α phase (decrease of the LAGB at the beginning of the deformation then increase at the last deformation level).

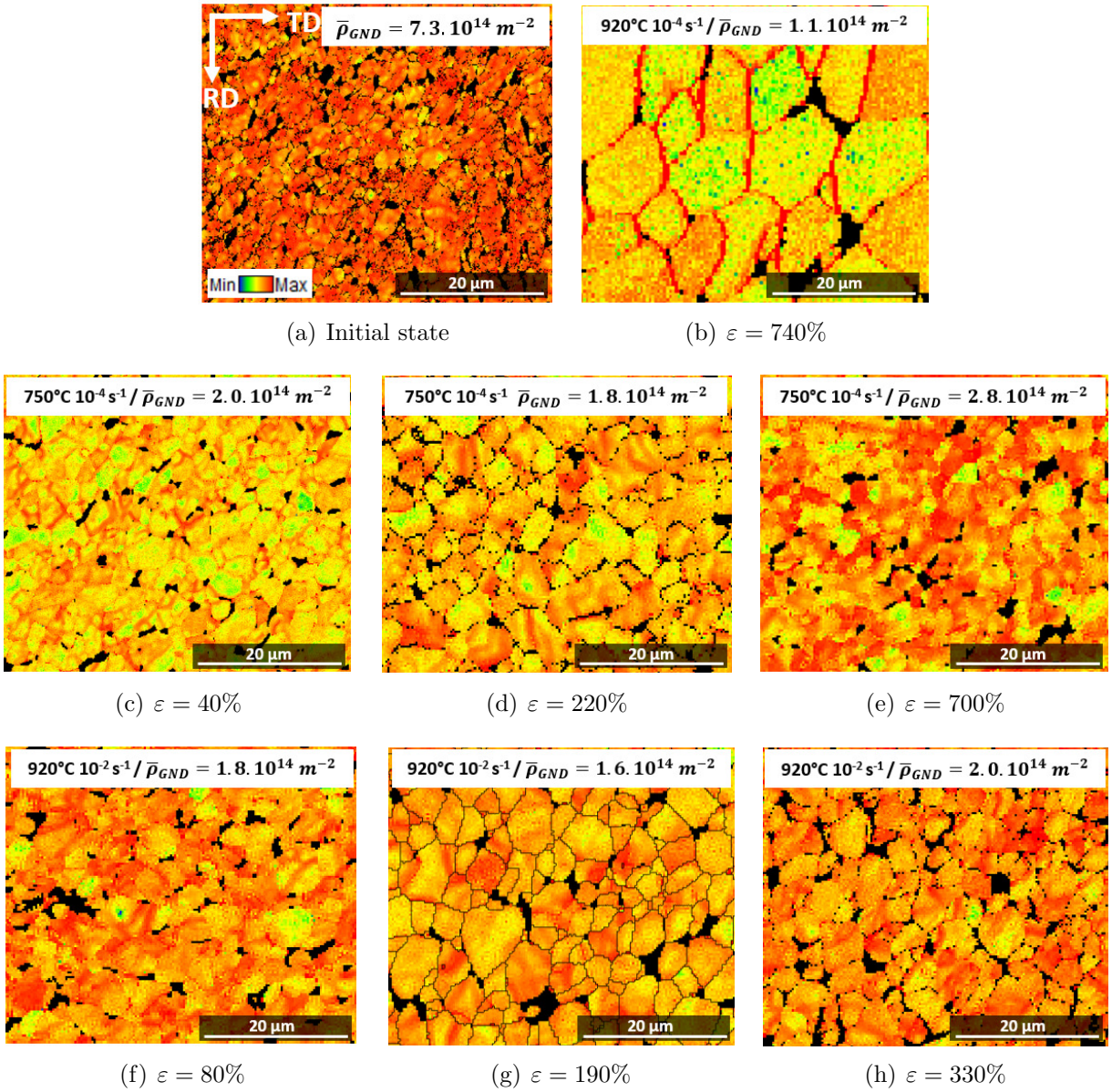

(a) Initial state (b) $\varepsilon = 740\%$

(c) $\varepsilon = 40\%$ (d) $\varepsilon = 220\%$ (e) $\varepsilon = 700\%$

(f) $\varepsilon = 80\%$ (g) $\varepsilon = 190\%$ (h) $\varepsilon = 330\%$

Figure 13: Dislocations density distribution: at the as-received state (a), at the last interrupted point at 920 °C 10^{-4} s^{-1} (b), at different deformation levels at 750 °C 10^{-4} s^{-1} (c-e) and 920 °C 10^{-2} s^{-1} (f-h). The mean value of geometrically necessary dislocations $\overline{\rho}_{\mathrm{GND}}$ obtained is shown on each map.

3.5. Kinetics analysis of the deformation

The deformation behaviour with a larger range of temperatures and strain rates conditions was then characterized according to kinetic analysis [29]. The values of strain rate sensitivity (m) reported in Table 1 were estimated at a plastic strain of 0.4 from different tensile tests carried out at three constant strain rates (10^{-2} s^{-1}, 10^{-3} s^{-1}, 10^{-4} s^{-1}) and four temperatures (750 °C, 870 °C, 900 °C, 920 °C), as shown on Fig.14. According to the literature [4], the mechanical behaviour is superplastic when the m value is greater than or equal to 0.3. Indeed,

the strain rate sensitivity represents the capacity of the material to resist necking and so to provide interesting deformation stability. Note that the m values of the superplastic material are mainly between 0.4 and 0.8 [30].

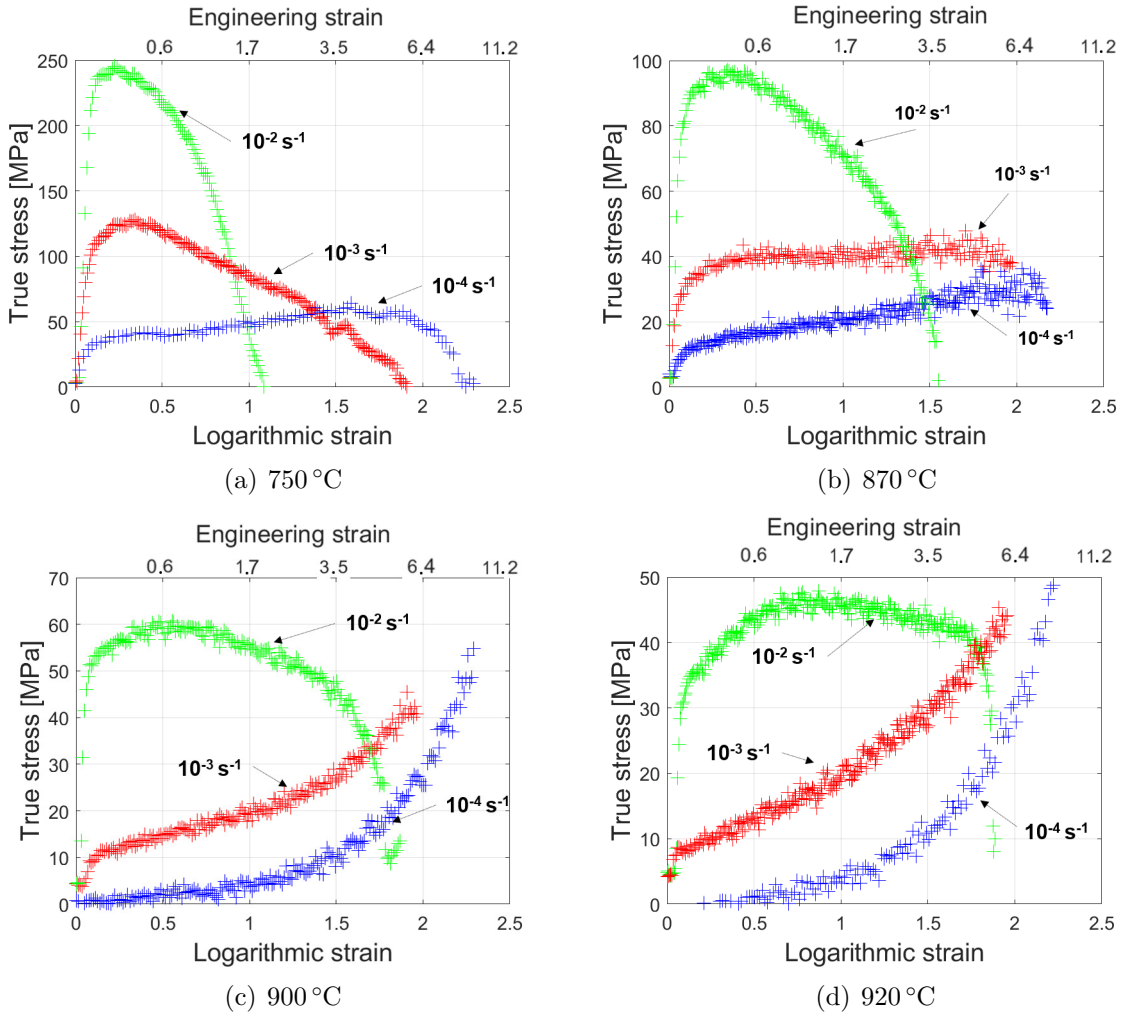

(a) 750 °C (b) 870 °C

(c) 900 °C (d) 920 °C

Figure 14: True stress and logarithmic strain curves obtained after tensile tests at 750 °C (a), 870 °C (b), 900 °C (c) and 920 °C (d) following three strain rates: $10^{-2}\,s^{-1}$, $10^{-3}\,s^{-1}$ and $10^{-4}\,s^{-1}$.

The estimated m values are higher than 0.3 regardless of the temperature, indicating that these conditions are favourable to superplastic behaviour. In addition, the value of m increases with temperature, which indicates the increase in GBS activity with temperature [29]. This observation can also be done on the Fig.14. Indeed by increasing the temperature, high elongations are reached even for high strain rates. Warren et al. [31] describe an accommodation of the GBS by dislocations motion for $m = 0.5$ and an accommodation by grain boundary diffusion for $m = 1$. Regarding the values estimated here, it is possible to expect to find some dislocations activity for the lowest temperatures while for the highest, a diffusion phenomenon.

The apparent activation energy was estimated by assuming that the strain rate follows an Arrhenius-type equation (Eq.3).

$$\dot{\varepsilon} = A\sigma^n exp(-\frac{Q}{RT}) \tag{3}$$

Where A is the material constant, R the gas constant ($8.314\,\mathrm{J\,mol^{-1}\,K^{-1}}$), T the temperature (K) and $n = \frac{1}{m}$ is the stress exponent. Estimated apparent activation energy values are reported in Table 1. Moreover, Table.1 shows a decrease of the Q values from 750 °C to 920 °C, the value is three times higher at low temperature than at high temperature, suggesting that specific deformation and accommodation mechanisms are involved by increasing the temperature and so the "soft"-β phase fraction [32]. The estimated Q values are close to the reported ones (Table.2). For the lowest temperatures, the mechanism could be controlled by GBS with dislocations motion and dynamic recrystallization. At 870 °C, the mechanism, reported in the literature with a Q value close to the estimated Q, would be GBS with lattice diffusion involving the α phase. At highest temperatures, the mechanism would be volume self-diffusion in the β phase with a Q value lower than $200\,\mathrm{kJ\,mol^{-1}}$.

Temperature (°C)	m	Q ($\mathrm{kJ\,mol^{-1}}$)
750	0.33	436
870	0.55	259
900	0.73	196
920	0.82	175

Table 1: Summary of strain rate sensitivity (m) and activation energy (Q) for a plastic strain of 0.4 and following different temperatures.

Activation energy Q ($\mathrm{kJ\,mol^{-1}}$)	**Reported deformation mechanisms**
121-132	Grain boundary self-diffusion for an α Ti [12, 33]
170	Self-diffusion for a Ti-6Al-4V alloy in β region [32]
184-188	GBS accommodated by dislocation slip/creep mechanism [34]
242-264	Nabarro-Herring creep, volume diffusion for an α titanium alloy [12, 33]
522	Dynamic recrystallization in α+β region [32]

Table 2: Summary of activation energy reported in the literature.

The Zener-Hollomon parameter (Z) represents the temperature-compensated strain rate parameter used for kinetics analysis and defined as follows:

$$Z = \dot{\varepsilon} \exp \frac{Q}{RT} \tag{4}$$

Where R is the gas constant ($8.314\,\mathrm{J\,mol^{-1}\,K^{-1}}$), $\dot{\varepsilon}$ is the strain rate applied during the tensile test ($\mathrm{s^{-1}}$), T is the temperature (K) and Q the apparent activation energy ($\mathrm{kJ\,mol^{-1}}$).

Fig.15 represents the evolution of the stress for the plastic strain of 0.4 ($\log(\sigma_{0.4})$) as a function of the log(Z). This relationship, obtained with the Eq.1 and 4, is almost linear for the highest strain rate, which means the deformation is a thermally activated process [29]. Moreover there is a modification of the deformation mechanisms involved according to the associated strain rate because a modification of the slope can be observed with the evolution of the Z parameter. An overlap of two σ values can be observed at $\log(Z) = 9.8$. These points correspond to a temperature of 750 °C and 920 °C for different strain rates but corresponds to the same stress level. This means that the active deformation mode is similar. It is also remarkable that one of the points has a stress value quite distant from the other conditions (right corner Fig.15). This would mean that the GBS mechanism would not be activated under these conditions. The m values higher than 0.3 were obtained for all conditions but with different activation energies which means that the deformation mechanisms involved should be different for each condition.

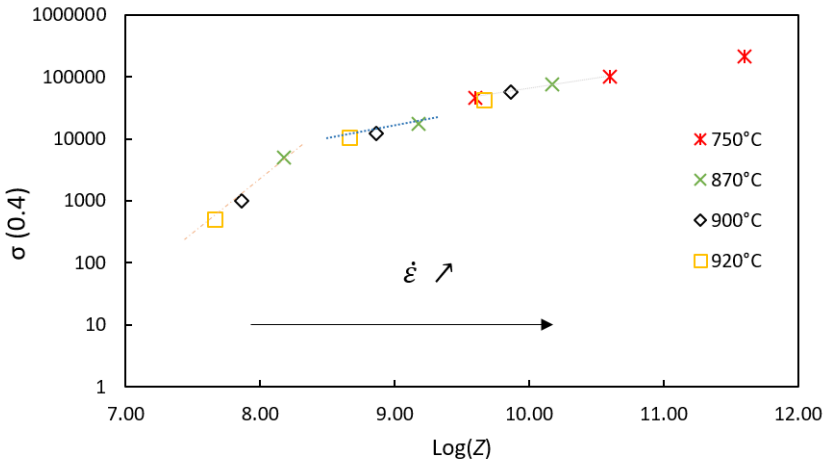

Figure 15: $\sigma_{0.4}$ in log scale as a function of $\log(Z)$ illustrating a large variation of Z parameter with the temperature.

4. Discussion

As previously introduced, it is widely reported that the superplastic mechanisms in two-phase titanium alloys are mainly related to grain boundary sliding accommodated by dislocations slip/creep and/or diffusion. In particular, it is supposed that most of the accommodation mechanisms are carried out by the β phase, which has larger number of slip systems and a higher atomic diffusivity than α. These mechanisms can change with increasing the strain. Moreover, microstructural evolution by dynamic recovery, recrystallization and/or grain growth are often observed. This study, on the mechanical behaviour at high temperature of a fine-grained Ti-6Al-4V alloy, revealed that this alloy exhibits different changes in

deformation mechanisms depending on the temperature and the strain rate. Indeed these changes are highlighted by the mechanical behaviour evolution, the values of both the strain rate sensitivity and the activation energy that can be related to microstructural and micro-textural modifications which are the grain size, grain shape, phase fraction and texture.

First of all, by comparing these experimental results with those obtained for Ti-6Al-4V currently used for superplastic forming (i.e. with an α grain size around 10 µm [2]), it can be confirmed that by decreasing the size of the α nodules, the superplastic behaviour at 750 °C is improved. However, by increasing the strain rate, the steady-state flow characteristic of superplastic behaviour seems to be favoured by an increase in temperature (Fig.6(a)).

At low temperature (750 °C) and high strain rate ($10^{-2}\,s^{-1}$), the studied alloy exhibits a strain rate sensitivity parameter m higher than 0.3 and an elongation of 250% which is lower than that of superplastic materials (> 300%). These two parameters indicate that the superplastic effect is probably weak. Moreover the activation energy value calculated (Q=436 kJ mol^{-1}) is clearly higher than activation energy involving self-diffusion mechanisms [17, 35] and tends to values linked to dynamic recrystallization which is generally associated with the dislocations activity/storage. The softening shown before failure is similar to the behaviour reported in the literature [14, 25] that is related to dislocations activity. Thus, the mechanism controlling the deformation, at low temperature and high strain rate seems not to be mainly related to GBS but rather to the dislocations activity leading to the continuous dynamic recrystallization (CDRX) (as noticed with the decrease of both the LAGB fraction and α phase grain size) [14, 36]. Moreover, regardless of the deformation level at 750 °C, a decrease of the overall texture intensity associated to a change of the crystallographic orientation of $\{0001\}_\alpha$ basal planes is observed and can be also related to dislocations activity within α grains (Fig.10(c)). Indeed, it is mainly reported that grain rotation accompanied by GBS leads to a homogeneous randomization of the preferred orientation [37] while intragranular dislocations activity would be more consistent with texture changes [38].

On the contrary, for the highest temperature and the lowest strain rate (920 °C $10^{-4}\,s^{-1}$), the alloy shows a high elongation (740%) associated to a high m value (0.82) and a low apparent activation energy (Q=175 kJ mol^{-1}) that should evidence an interesting superplastic behaviour. We can noticed that the m value is higher than the value obtained by Alabort et al. for a grain size of 6 µm [15], which highlights the impact of the initial grain size on the behaviour of the material. Even if the alloy exhibits an initial low flow stress, an important hardening is noticed by increasing the strain. The high temperature associated to the low strain and the hardening make thus the forming of this alloy in these conditions both expensive and inefficient. It is important to notice, that contrary to what it is usually mentioned in the literature, the high hardening behaviour can not be explained in totality by the α grain growth. Indeed, in the FG titanium alloy, the α grain growth occurred mainly in the early deformation stage (Fig.7), whereas the flow stress highly increases over an elongation of 420%. So it is believed that other changes at the microstructural level, in addition to the α grain growth, should be involved in this hardening. In particular, at 920 °C, it is important to remind that the β phase fraction (52 vol.%) is almost equivalent to the α phase fraction (48 vol.%). Moreover as the alloying elements diffusivity in the β phase is two times faster than

in the α phase, the high temperature microstructure can thus be considered as composed by non-deformable α grains surrounded by deforming β phase [38, 39]. As a result, increasing the distance between α grains and changing the spatial distribution of the two phases result in a significant change of the number and type of interfaces (α/β, α/α, β/β). It can be assumed a lower occurrence of GBS mechanism with the decrease of the area fraction of α/β interfaces favourable to GBS [9] as the sliding resistance of α/α and β/β boundaries are reported to be higher than α/β interfaces. Nevertheless, at 920 °C, the post-mortem SEM observations cannot highlight any microstructural changes in β due to the slow cooling applied. At this high temperature (920 °C), the small KAM dispersion obtained (Fig.12(b) and (d)), associated to a strong decrease of the average KAM value suggests that there are few local defects in the α phase and that the deformation is clearly controlled by the β phase. Indeed the β phase having a rather high stacking fault energy and a high diffusivity, it will favour both, the reduction of the dislocations density during deformation by dynamic recovery [11, 40] and also bulk diffusion mechanisms that, at low strain rate, can easily lead to dynamic coarsening in β and so to changes of the number of β/β interfaces. Judging from the values of the activation energy as well as the results of the microstructural observations, it would appear that the predominant deformation mechanism may be supported by the β phase, like a volume self diffusion and a diffusion at interfaces (α/β or β/β), favoured by the high temperature and the low strain rate applied.

One interesting result in this study concerns the similar flow behaviour observed for two different conditions of temperature and strain rate (750 °C $10^{-4}\,s^{-1}$ and 920 °C $10^{-2}\,s^{-1}$) on Fig.6. Indeed, a superplastic flow behaviour with a similar stress level (about 45 MPa) was noticed for these two conditions. However, as previously explained, at these two temperatures (750 °C and 920 °C), the α and β phases fractions, the strain rate sensitivity m as well as the apparent activation energy Q are distinctly different implying that the mechanisms of deformation operating are not the same even if there are similarities of flow behaviour. Note also that at 920 °C $10^{-2}\,s^{-1}$ the alloy exhibits a lower elongation and a more stable flow behaviour than at 750 °C $10^{-4}\,s^{-1}$.

At low temperature (750 °C) and low strain rate, the deformation will be mainly controlled by the α phase as its volume phase fraction is around 88%. The steady state flow characteristics of superplastic flow observed and the m value of 0.33 calculated could be representative of GBS activation. At the first deformation step, microstructural studies reveal that the alloy has more equiaxed grain and more HAGBs than before deformation, which can be attributed to an initial poligonization process by dynamic recrystallization. This refined microstructure (with sufficient homogeneous β phase distributed around α grains) could promote GBS activation [41] by increasing the strain. Moreover, no modification of local plasticity in the α phase was shown (Fig.12(c)), which could highlight that the predominant deformation mechanism would be GBS with accommodation by dislocations motion at grain boundaries α/β. By comparison with the work of Alabort et al. [15], for an α grain size of 6 µm and a temperature of 700 °C, the β phase was not suitable to accommodate the deformation (cavities formation at interfaces). However, in our study, a β phase fraction of 12%, associated to a higher number of grain boundaries (due to a lower α grain size than in

the work of Alabort et al. [15]) seems quite appropriated. The increase of the α grains size shown at a stress level of 220% could induce the slight hardening noticed for this stress level. Indeed, at this slow strain rate, the dynamic coarsening can occur more readily during the longer deformation time. Finally, a dislocation activity favoured in the larger α grain, at the end of the deformation, could explain the change in the preferential orientation of grains as well as the increase in dislocations density.

Regarding the 920 °C $10^{-2}\,s^{-1}$ condition, the higher β phase fraction present at this temperature suggests that the mechanisms will mainly involve the β phase. Nevertheless, the high strain rate should prevent high diffusion mechanisms from occurring into β compared to a slow strain rate. Even if the α phase will play the role of inclusion in a soft β phase during the deformation, the stresses will be mainly localized at the β/β grain boundaries (Fig.13(f)) and thus lead to their motion. This mechanism corresponds to the GBS accommodated by the alloy elements diffusion [37]. Indeed the first step to accommodate the deformation is the alloy elements diffusion from either the core mantle or from the β grain leading then to the grain boundaries motion. The main deformation will be thus the GBS accommodated by diffusion in the β phase. This hypothesis is moreover confirmed thanks to the pole figures obtained by EBSD (Fig.10(g), 10(h) and 10(i)), which show that the texture in the α phase does not change much except at the failure. Indeed due to the high strain rate applied, the diffusion in the β phase is limited. The stress is then undergone by the α phase through the dislocations motion leading to the dynamic recrystallization in the α phase, as observed for the condition at 750 °C $10^{-4}\,s^{-1}$. If we compare our experimental observations as well as the calculated activation energies with those obtained in the literature, it would appear that the mechanisms described are quite similar [33, 34]. In consequence of these two conditions (750 °C $10^{-4}\,s^{-1}$ and 920 °C $10^{-2}\,s^{-1}$), the alloy has similar stress levels but the deformation mechanisms are respectively activated and accommodated by different energy levels and phenomena (dislocation motion, diffusion).

5. Conclusions

In this contribution, high temperature deformation mechanisms of the as-received Ti-6Al-4V titanium alloy with an α grain size of 2 µm were investigated by interrupted tensile tests and SEM/EBSD for two significantly different temperatures (750 °C and 920 °C) and two strain rates ($10^{-2}\,s^{-1}$ and $10^{-4}\,s^{-1}$). The following conclusions have been made:

1. Superplastic behaviour was obtained at low temperature (750 °C) and low strain rate ($10^{-4}\,s^{-1}$).
2. The microstructural observations at different steps of deformation at 750 °C $10^{-4}\,s^{-1}$ showed a complex evolution leading to the activation of different deformation mechanisms by increasing the strain. At first, a rearrangement of dislocations leads to the formation of nodular α grains followed by the activation of GBS accommodated by dislocations in smaller α nodules and in the β phase. Thereafter, a slight hardening was observed explained by an increase of the α grains size. Finally, a continuous dynamic

recrystallization is activated due to an accumulation of stress in the α phase. The deformation is mainly controlled by the α phase and accommodated by the surrounding β phase.

3. The superplastic behaviour, also obtained at high temperature (920 °C) and for a high strain rate ($10^{-2}\,s^{-1}$), is attributed to the activation of different deformation mechanisms than at 750 °C. In particular, the GBS seems to be the main mechanism of deformation but accommodated differently at 750 °C and 920 °C. While at 750 °C, the accommodation can be by dislocations glide at α/β interfaces and in some α grains, at 920 °C, the deformation is assumed to be accommodated by the β/β grain boundaries motion favoured by the alloy elements diffusivity in β.
4. At 920 °C $10^{-4}\,s^{-1}$, a high hardening was obtained with a superplastic elongation. These high hardening cannot be only explained by the grain growth observed. Regarding the activation energy and the texture evolution, a main mechanism in the β phase can be expected, like volume self-diffusion [32] and diffusion at α/β and β/β interfaces. Indeed at this temperature, there is a huge change of the number of α/β interfaces due to an increase of the β phase fraction which is in favour of a deformation supported by the β phase.
5. At 750 °C and 920 °C, the deformation mechanisms are mainly controlled by respectively the α phase and the β phase.

Acknowledgements

This study was funded by IMT Mines Albi and supported by Airbus France by supplying the initial sheets.

References

[1] C. Leyens, M. Peters, Titanium and Titanium Alloys: Fundamentals and Applications (2003). doi:10.1002/3527602119.

[2] J.-J. Blandin, M. SUERY, Superplasticité, Techniques de l'ingénieur Mise en forme des métaux : aspects rhéologiques et métallurgiques base documentaire : TIB476DUO. (ref. article : m613), publisher: Editions T.I. Type: base documentaire _eprint: base documentaire : TIB476DUO. (1996).
URL https://www.techniques-ingenieur.fr/base-documentaire/materiaux-th11/mise-en-forme-des-metaux-aspects-rheologiques-et-metallurgiques-42476210/superplasticite-m613/

[3] T. Zhang, Y. Liu, D. G. Sanders, B. Liu, W. Zhang, C. Zhou, Development of fine-grain size titanium 6Al–4V alloy sheet material for low temperature superplastic forming, Materials Science and Engineering: A 608 (2014) 265 – 272. doi:https://doi.org/10.1016/j.msea.2014.04.098.
URL http://www.sciencedirect.com/science/article/pii/S0921509314005620

[4] S. Semiatin, T. Bieler, The effect of alpha platelet thickness on plastic flow during hot working of TI–6Al–4V with a transformed microstructure, Acta Materialia 49 (17) (2001) 3565–3573. doi:10.1016/S1359-6454(01)00236-1.
URL http://www.sciencedirect.com/science/article/pii/S1359645401002361

[5] E. Alabort, D. Barba, M. R. Shagiev, M. A. Murzinova, R. M. Galeyev, O. R. Valiakhmetov, A. F. Aletdinov, R. C. Reed, Alloys-by-design: Application to titanium alloys for optimal superplasticity, Acta Materialia 178 (2019) 275 – 287. doi:https://doi.org/10.1016/j.actamat.2019.07.026.
URL http://www.sciencedirect.com/science/article/pii/S1359645419304665

[6] H. Matsumoto, K. Yoshida, S.-H. Lee, Y. Ono, A. Chiba, Ti–6Al–4V alloy with an ultrafine-grained microstructure exhibiting low-temperature–high-strain-rate superplasticity, Materials Letters 98 (2013) 209 – 212. doi:https://doi.org/10.1016/j.matlet.2013.02.033.
URL http://www.sciencedirect.com/science/article/pii/S0167577X13002127

[7] S. Zherebtsov, E. Kudryavtsev, G. Salishchev, B. Straumal, S. Semiatin, Microstructure evolution and mechanical behavior of ultrafine Ti6Al4V during low-temperature superplastic deformation, Acta Materialia 121 (2016) 152–163. doi:10.1016/j.actamat.2016.09.003.
URL http://www.sciencedirect.com/science/article/pii/S1359645416306814

[8] M. Vanderhasten, L. Rabet, B. Verlinden, Ti–6Al–4V: Deformation map and modelisation of tensile behaviour, Materials & Design 29 (6) (2008) 1090 – 1098. doi:https://doi.org/10.1016/j.matdes.2007.06.005.
URL http://www.sciencedirect.com/science/article/pii/S0261306907001665

[9] J. S. Kim, J. H. Kim, Y. T. Lee, C. G. Park, C. S. Lee, Microstructural analysis on boundary sliding and its accommodation mode during superplastic deformation of Ti–6Al–4V alloy, Materials Science and Engineering: A 263 (2) (1999) 272 – 280. doi:https://doi.org/10.1016/S0921-5093(98)01157-5.
URL http://www.sciencedirect.com/science/article/pii/S0921509398011575

[10] M. L. Meier, D. R. Lesuer, A. K. Mukherjee, Alpha Grain size and beta volume fraction aspects of the superplasticity of Ti-6Al-4V, Materials Science and Engineering: A 136 (1991) 71 – 78. doi:https://doi.org/10.1016/0921-5093(91)90442-P.
URL http://www.sciencedirect.com/science/article/pii/092150939190442P

[11] M. Zhou, F. P. E. Dunne, Mechanisms-based constitutive equations for the superplastic behaviour of a titanium alloy, The Journal of Strain Analysis for Engineering Design 31 (3) (1996) 187–196. doi:10.1243/03093247V313187.
URL https://doi.org/10.1243/03093247V313187

[12] K. Janghorban, S. Esmaeili, Deformation-mechanism map for Ti-6Al alloy, Journal of Materials Science 26 (12) (1991) 3362–3365. doi:10.1007/BF01124686.
URL https://doi.org/10.1007/BF01124686

[13] M. Motyka, J. Sieniawski, W. Ziaja, Microstructural aspects of superplasticity in Ti–6Al–4V alloy, Materials Science and Engineering: A 599 (2014) 57 – 63. doi:https://doi.org/10.1016/j.msea.2014.01.067.
URL http://www.sciencedirect.com/science/article/pii/S0921509314000987

[14] H. S. Yang, G. Gurewitz, A. K. Mukherjee, Mechanical Behavior and Microstructural Evolution during Superplastic Deformation of Ti–6Al–4V, Materials Transactions, JIM 32 (5) (1991) 465–472. doi:10.2320/matertrans1989.32.465.

[15] E. Alabort, P. Kontis, D. Barba, K. Dragnevski, R. Reed, On the mechanisms of superplasticity in Ti–6Al–4V, Acta Materialia 105 (Supplement C) (2016) 449–463. doi:10.1016/j.actamat.2015.12.003.
URL http://www.sciencedirect.com/science/article/pii/S1359645415301105

[16] S. L. Semiatin, M. W. Corbett, P. N. Fagin, G. A. Salishchev, C. S. Lee, Dynamic-coarsening behavior of an alpha/beta titanium alloy, Metallurgical and Materials Transactions A 37 (4) (2006) 1125–1136. doi:10.1007/s11661-006-1091-x.
URL https://doi.org/10.1007/s11661-006-1091-x

[17] C. Liu, G. Zhou, X. Wang, J. Liu, J. Li, H. Zhang, L. Chen, Rheological Law and Mechanism for Superplastic Deformation of Ti–6Al–4V, Materials 12 (21) (2019). doi:10.3390/ma12213520.
URL https://www.mdpi.com/1996-1944/12/21/3520

[18] A. W. Bowen, Texture stability in heat treated Ti6Al4V, Materials Science and Engineering 29 (1) (1977) 19 – 28. doi:https://doi.org/10.1016/0025-5416(77)90141-0.
URL http://www.sciencedirect.com/science/article/pii/0025541677901410

[19] S. I. Wright, M. M. Nowell, D. P. Field, A Review of Strain Analysis Using Electron Backscatter Diffraction, Microscopy and Microanalysis 17 (3) (2011) 316–329. doi:10.1017/S1431927611000055.

[20] N. Saunders, R. W. Cahn, M. McLean, M. Rappaz, D. G. Pettifor, Phase Diagram Calculations for High-Temperature Structural Materials, Philosophical Transactions: Physical Sciences and Engineering 351 (1697) (1995) 543–561.
URL www.jstor.org/stable/54492

[21] J.-O. Andersson, T. Helander, L. Höglund, P. Shi, B. Sundman, Thermo-Calc & DICTRA, computational tools for materials science, Calphad 26 (2) (2002) 273 – 312. doi:https://doi.org/10.1016/S0364-5916(02)00037-8.
URL http://www.sciencedirect.com/science/article/pii/S0364591602000378

[22] S. Malinov, P. Markovsky, W. Sha, Z. Guo, Resistivity study and computer modelling of the isothermal transformation kinetics of Ti–6Al–4V and Ti–6Al–2Sn–4Zr–2Mo–0.08Si alloys, Journal of Alloys and Compounds 314 (1) (2001) 181–192. doi:10.1016/S0925-8388(00)01227-5.
URL http://www.sciencedirect.com/science/article/pii/S0925838800012275

[23] J. Elmer, T. Palmer, S. Babu, E. Specht, In situ observations of lattice expansion and transformation rates of alpha and beta phases in Ti–6Al–4V, Materials Science and Engineering: A 391 (1) (2005) 104–113. doi:10.1016/j.msea.2004.08.084.
URL http://www.sciencedirect.com/science/article/pii/S0921509304011232

[24] M. Dehmas, R. Katemi, B. Appolaire, E. Aeby-Gautier, B. Denand, S. Audion, Dissolution kinetics of alpha phase in TA6V titanium alloy, in: Ti 2011 - Proceedings of the 12th World Conference on Titanium, Vol. 1, 2011.
URL https://www.researchgate.net/publication/234057726

[25] E. Alabort, D. Putman, R. Reed, Superplasticity in Ti–6Al–4V: Characterisation, modelling and applications, Acta Materialia 95 (Supplement C) (2015) 428–442. doi:10.1016/j.actamat.2015.04.056.
URL http://www.sciencedirect.com/science/article/pii/S1359645415003080

[26] S. Semiatin, V. Seetharaman, I. Weiss, Flow behavior and globularization kinetics during hot working of Ti–6Al–4V with a colony alpha microstructure, Materials Science and Engineering: A 263 (2) (1999) 257–271. doi:10.1016/S0921-5093(98)01156-3.
URL http://www.sciencedirect.com/science/article/pii/S0921509398011563

[27] F. Léaux, Relation entre microstructure et fatigue d'un acier ferritique utilisé dans l'industrie automobile : élaboration d'indicateurs d'endommagement, PhD Thesis (2012).
URL http://www.theses.fr/2012LIL10112/document

[28] M. F. Ashby, The deformation of plastically non-homogeneous materials, The Philosophical Magazine: A Journal of Theoretical Experimental and Applied Physics 21 (170) (1970) 399–424. doi:10.1080/14786437008238426.
URL https://doi.org/10.1080/14786437008238426

[29] H. Imai, G. Yamane, H. Matsumoto, V. Vidal, V. Velay, Superplasticity of metastable ultrafine-grained Ti6242S alloy: Mechanical flow behavior and microstructural evolution, Materials Science and Engineering: A 754 (2019) 569 – 580. doi:https://doi.org/10.1016/j.msea.2019.03.085.
URL http://www.sciencedirect.com/science/article/pii/S0921509319303983

[30] J. Pilling, Superplasticity in Crystalline Solids, The Institute of Metals (1989) 175–178.
URL https://ci.nii.ac.jp/naid/10004208640/en/

[31] J. Warren, L. M. Hsiung, H. N. G. Wadley, High temperature deformation behavior of physical vapor deposited Ti-6Al-4V, Acta Metallurgica et Materialia 43 (7) (1995) 2773 – 2787. doi:https://doi.org/10.1016/0956-7151(94)00464-S.
URL http://www.sciencedirect.com/science/article/pii/095671519400464S

[32] T. Sheppard, J. Norley, Deformation characteristics of Ti–6Al–4V, Materials Science and Technology 4 (10) (1988) 903–908. doi:10.1179/mst.1988.4.10.903.
URL https://doi.org/10.1179/mst.1988.4.10.903

[33] G. Malakondaiah, P. R. Rao, Creep of Alpha-Titanium at low stresses, Acta Metallurgica 29 (7) (1981) 1263 – 1275. doi:https://doi.org/10.1016/0001-6160(81)90017-1.
URL http://www.sciencedirect.com/science/article/pii/0001616081900171

[34] A. V. Mikhaylovskaya, A. O. Mosleh, A. D. Kotov, J. S. Kwame, T. Pourcelot, I. S. Golovin, V. K. Portnoy, Superplastic deformation behaviour and microstructure evolution of near-alpha Ti-Al-Mn alloy, Materials Science and Engineering: A 708 (2017) 469 – 477. doi:https://doi.org/10.1016/j.msea.2017.10.017.
URL http://www.sciencedirect.com/science/article/pii/S0921509317313357

[35] A. Arieli, A. Rosen, Superplastic deformation of Ti-6Al-4V alloy, Metallurgical Transactions A 8 (10) (1977) 1591–1596. doi:10.1007/BF02644864.
URL https://doi.org/10.1007/BF02644864

[36] K. Huang, R. E. Logé, A review of dynamic recrystallization phenomena in metallic materials, Materials & Design 111 (2016) 548 – 574. doi:https://doi.org/10.1016/j.matdes.2016.09.012.
URL http://www.sciencedirect.com/science/article/pii/S0264127516311753

[37] M. F. Ashby, R. A. Verrall, Diffusion-accommodated flow and superplasticity, Acta Metallurgica 21 (2) (1973) 149 – 163. doi:https://doi.org/10.1016/0001-6160(73)90057-6.
URL http://www.sciencedirect.com/science/article/pii/0001616073900576

[38] D. S. McDarmaid, P. G. Partridge, The effect of strain rate, temperature and texture on anisotropic deformation in Ti-6Al-4V, Journal of Materials Science 21 (5) (1986) 1525–1532. doi:10.1007/BF01114705.
URL https://doi.org/10.1007/BF01114705

[39] P. G. Partridge, D. S. McDarmaid, A. W. Bowen, A deformation model for anisotropic superplasticity in two phase alloys, Acta Metallurgica 33 (4) (1985) 571 – 577. doi:https://doi.org/10.1016/0001-6160(85)90021-5.
URL http://www.sciencedirect.com/science/article/pii/0001616085900215

[40] P. M. Souza, H. Beladi, R. Singh, B. Rolfe, P. D. Hodgson, Constitutive analysis of hot deformation behavior of a Ti6Al4V alloy using physical based model, Materials Science and Engineering: A 648 (2015) 265–273. doi:10.1016/j.msea.2015.09.055.
URL http://www.sciencedirect.com/science/article/pii/S0921509315303907

[41] Z. X. Zhang, S. J. Qu, A. H. Feng, J. Shen, D. L. Chen, Hot deformation behavior of Ti-6Al-4V alloy: Effect of initial microstructure, Journal of Alloys and Compounds 718 (2017) 170 – 181. doi:https://doi.org/10.1016/j.jallcom.2017.05.097.
URL http://www.sciencedirect.com/science/article/pii/S0925838817316808